

Sensitivity Analysis of Pulsatile Hydromagnetic Biofluid Flow and Heat Transfer with Non Linear Darcy-Forchheimer Drag

S. Rawat¹, R. Bhargava², S. Kapoor³ and S. Sharma^{4†}

¹Department of General Studies (Mathematics group), Jubail University College, Jubail, Saudi Arabia, E-mail: sam.rawat@gmail.com

²Department of Mathematics, Indian Institute of Technology, Roorkee - 247667, India.
E-mail rbharmfa@iitr.ernet.in

³Department of Education in Science and Mathematics, Regional Institute of Education, Bhubneswar
(NCERT), India, E-mail: saurabh09.iitr@gmail.com

⁴Department of Mathematics, DAV University College, Jalandhar, India

†Corresponding Author Email:sapna2002@gmail.com

(Received September 29, 2014; accepted June 16, 2015)

ABSTRACT

In the present paper we examine the pulsatile hydromagnetic flow and heat transfer of a non-Newtonian biofluid through a saturated non-Darcian porous medium channel. The upper plate of the channel is heated and the lower plate is cooled. The Nakamura-Sawada rheological model is employed which provides a higher yield stress than the Casson model. A Darcy-Forchheimer porous medium drag force model is incorporated to simulate blood vessel blockage with deposits in the cardiovascular system. Viscous heating is also included in the energy equation. The governing conservation equations for mass, momentum and energy equation are transformed into a system of nonlinear, coupled ordinary differential equations and these are solved numerically using finite element method. The effect of other important parameters such as magnetohydrodynamic parameter (N_m), Reynolds number (Re), Eckert number (Ec), Darcian parameter (λ), Forchheimer parameter (N_F) and Prandtl number on velocity and temperature profiles are studied graphically. Spatial-temporal velocity and temperature profile visualizations are also presented. Numerical results shows that normalized fluid velocity (U) increases throughout the channel ($-1 < Y < 1$) with an increase in Reynolds number, Darcian parameter, steady pressure gradient parameter and rheological parameter; conversely velocity is decreased with the increase in magnetic parameter and Forchheimer quadratic drag parameter. Higher Eckert number ($Ec = 3$) is also found to have a considerable effect on temperature (θ) profile. Finite difference numerical computations are also compared with the finite element solutions to verify efficiency and accuracy.

Keywords: Magneto-hydrodynamic; Porous media; Rheology; Heat transfer; Pulsatile; Numerical, Eckert number.

1. INTRODUCTION

Physiological fluid dynamics in the presence of applied magnetic fields has developed into a significant area of interest in the engineering sciences over the past decade owing to rapid technological progress in medical applications concerning the control of blood flow during surgical operations, human circulation system response to electromagnetic fields (in the vicinity of power cables) and also drug targeting innovations. Tenforde (2005) studied numerically the hydromagnetic aortic model showing that magnetohydrodynamic interactions reduce the volume flow rate of blood in the human aorta.

These magneto-hemodynamic studies used the Newtonian i.e. Navier-Stokes flow model. The complex rheological nature of physiological fluids such as blood, bile, mucus, semen and so forth, can however not been recognized using Newtonian models. Numerous investigations have established that blood behaves as a Non-Newtonian fluid at low shear rates. Chattopadhyay *et al.* (2006) studied using the SIMPLE numerical algorithm, the laminar flow and heat transfer in a circular tube under pulsating flow condition. Several studies have also addressed the pulsatile blood flows with heat transfer. Soon after wards Ogulu (2006) analyzed heat generation effects on hydromagnetic flow and species diffusion in a lymphatic blood

vessel. Later, Misra *et al.* (2008) investigated numerically the steady incompressible hydromagnetic blood flow and heat transfer in a parallel plate channel with stretching walls using the Walter's B viscoelastic model. The above studies were all restricted to purely fluid regimes. In many aspects of biomechanics the transport medium may be porous. Important examples include the pulmonary system, perfused tissue, the renal system and also blood vessels containing fatty deposits and blockages (arterial disease). Khaled and Vafai (2003) have presented a rigorous review of heat and fluid dynamics applications in porous (biological) media. The Darcy model has generally been most widely implemented in porous biofluid mechanics. For example Bég *et al.* (2007b) investigated numerically the biomagnetic micropolar blood flow in a Darcian porous tissue medium, using a ferrohydrodynamic formulation extending previous non-porous, Newtonian studies by Loukopoulos and Tzirtzikakis (2004). Ogulu and Amos (2007) investigated the effects of temporally-varying wall mass flux on hydromagnetic pulsatile Newtonian blood flow in a Darcian porous model of the cardiovascular system, using a regular perturbation technique. Under higher pressure gradients and in highly porous regimes where inertial effects dominate viscous effects, the Darcian model flow is inadequate. The popular engineering approach to simulate drag forces experienced at higher velocities employs the Forchheimer extension to the Darcy model or the so-called *Darcy-Forchheimer drag model*. Several investigations of Darcy-Forchheimer porous media transport have appeared however in the context of blood flows, whether steady or pulsatile. In the mean time, Bhargava *et al.* (2007a) used a finite element technique to analyze pulsating magneto-hydrodynamic blood flow and species diffusion in a porous medium channel using the Darcy-Forchheimer model. The Newtonian biomagnetic flow of blood in a Darcy-Forchheimer porous regime was studied by Bég *et al.* (2007a). Bhargava. *et al.* (2007b) investigated the non-magnetic flow of fluid through a non-Darcian channel in the absence of heat transfer. In the past (2010) the authors have been focusing on the impact of viscous dissipation effects or thermal dissipation in Darcy-Forchheimer porous medium. Ghazian (2011) investigated analytically the impact of viscous dissipation in channel filled with porous medium and observed that the gap size between the porous region and the clear fluid directly affects the viscous dissipation due to change in the resistance of the fluid. In the recent past Islam (2012) has given an interesting result on unsteady pulsatile flow of blood through porous media. It was an analytical investigation using the laplace transform technique. Along with this study Nadeem (2012) had investigated the heat and mass transfer effects on Newtonian biogenetic flow of blood through porous media and it was basically related to the flow in artery with stenosis. Keeping in view the above literature our objective is to understand the impact of the above terminology while taking the non-Newtonian biofluid through channel filled with

porous medium. More specifically, in the present problem we study the pulsatile magneto-rheological blood flow and heat transfer under transverse magnetic field with viscous heating effects through a Darcy-Forchheimer porous medium channel cooled at the lower plate and heated at the upper, using the Nakamura-Sawada bi-viscosity non-Newtonian model. Such a study has to the authors' knowledge thus far not received attention in the scientific literature and find finds applications in magneto-hemodynamics, materials processing, heat transfer enhancement in industrial systems etc.

2. MATHEMATICAL FORMULATION

Consider the unsteady, two dimensional, laminar, incompressible, electrically-conducting pulsating, bio-rheological fluid flow between two parallel plates intercalating an isotropic, homogenous, saturated, Darcy-Forchheimer porous medium. The two plates are located at a distance $2H$ apart with reference to an (x, y) coordinate system, where x defines the longitudinal coordinate parallel to the plates and y the transverse coordinate, perpendicular to the wall. The lower plate is kept at temperature T_1 and upper plate at temperature T_2 such that $T_1 < T_2$. In the present model, the pulsatory character of the physiological flow is generated by a source at infinity, following the so called "pistons at infinity" approximation, as described by Majdalani and Chibli (2002) (the actual pulsatile flow is due to the pumping of the heart in the human cardiovascular system).

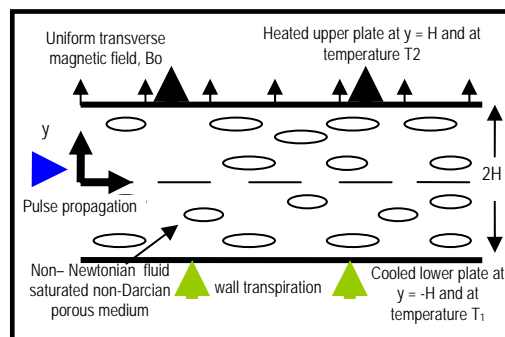


Fig. 1. Physical Model and Coordinate System.

The physical model is shown in fig. 1. In order to simulate the inertial drag effects imparted by the porous matrix in higher velocity flow, the Darcy-Forchheimer model is used. Magnetic Reynolds number is assumed to be small enough to neglect induced magnetic field effects and the applied magnetic field is uniform. The absence of an electrical field also allows exclusion of the effect of polarization of the ionized biofluid (blood). Joule heating effects are also ignored. Wall transpiration is present at both plates via injection at the lower plate ($y = -H$) and suction at the upper plate ($y = +H$). A stress tensor τ_{ij} is introduced into the momentum equation to take into account the

rheological characteristic of the blood. Following Nakamura and Sawada [8] we employ the bi-viscosity rheological model which is defined as follows:

$$\tau_{IJ} = \begin{cases} 2 \left[\mu_B + \frac{P_y}{\sqrt{2\pi}} \right] e_{ij}, & \pi > \pi_c \\ 2 \left[\mu_B + \frac{P_y}{\sqrt{2\pi_c}} \right] e_{ij}, & \pi < \pi_c \end{cases} \quad (1)$$

where $\pi = e_{ij} e_{ij}$ and e_{ij} is the $(i, j)^{th}$ component of the deformation rate, π_c is a critical value of this product based on the Nakamura-Sawada model, μ_B is plastic dynamic viscosity of the non-Newtonian fluid and P_y is yield stress of the fluid. Since the channel walls are infinitely long, the flow variables (velocity, temperature) are purely functions of y and τ . The system of equations governing the flow and energy is therefore given by:

Linear Momentum Equation:

$$\frac{\partial u}{\partial \tau} + V_0 \frac{\partial u}{\partial y} + \frac{1}{\rho} \frac{\partial P}{\partial x} = v_B \left(1 + \frac{1}{\beta} \right) \frac{\partial^2 u}{\partial y^2} - \frac{\sigma B_0^2}{\rho} u - \frac{v_B}{k_p} u - bu^2 \quad (2)$$

Energy (Heat) Equation:

$$\frac{\partial T}{\partial \tau} + V_0 \frac{\partial T}{\partial y} = \alpha \frac{\partial^2 T}{\partial y^2} + \frac{v_B}{k_p c_p} u^2 + \frac{b}{c_p} u^3 \quad (3)$$

The corresponding boundary conditions on the horizontal plate surfaces are:

$$y = -H: u = 0, T = T_1 \quad (4a)$$

$$y = H: u = 0, T = T_2 \quad (4b)$$

where μ is Newtonian dynamic viscosity, V_0 is wall transpiration velocity ($V = V_0$) at the lower plate and $V = -V_0$ at the upper plate), β denotes the upper limit of the apparent viscosity coefficient, where u is the x-direction (longitudinal velocity), P is the hydrodynamic pressure, μ is the dynamic viscosity, k_p is hydraulic conductivity (permeability) of the porous material, ρ is the density of the fluid, b is a Forchheimer (inertial drag) coefficient related to the porous medium geometry, τ is the dimensional time, σ is the electrical conductivity of the biofluid (assumed constant), B_0 is the transverse magnetic field strength, α is thermal diffusivity, c_p is the specific heat capacity of the biofluid, T denotes biofluid temperature and $\partial P/\partial x$ denotes longitudinal pressure gradient. Proceeding with the analysis we now normalize the flow model using the following transformations:

$$U = \frac{u}{V_0}, \quad X = \frac{x}{H}, \quad Y = \frac{y}{H}, \quad t = \frac{V_0}{H} \tau, \quad P^* = \frac{P}{\rho V_0^2}$$

$$\theta = \frac{T - T_m}{T_2 - T_m}, \quad Pr = \frac{v_B}{\alpha}, \quad Re = \frac{HV_0}{v_B}, \quad Nm = \frac{\sigma B_0^2 H}{\rho V_0}, \quad \lambda = \frac{k_p V_0}{v_B H}, \quad N_F = Hb, \quad Ec = \frac{V_0^2}{c_p (T_2 - T_m)},$$

where X and Y are dimensionless coordinates

parallel and transverse to the channel walls respectively, U is the transformed velocity component in the X -direction, P^* is the transformed hydrodynamic pressure (* dropped for convenience in analysis), t is dimensionless time, θ is dimensionless temperature, Re is a transpiration Reynolds number, Nm is the hydromagnetic parameter, λ is a Darcian (permeability) parameter, N_F is the Forchheimer (quadratic porous drag) parameter, $T_m = \frac{T_1 + T_2}{2}$ is the characteristic temperature, Pr is the Prandtl number and Ec is the Eckert Number. Introducing (5) into equations (1)-(3) leads to the following set of non-linear, coupled, ordinary differential equations:

Momentum Equation:

$$\frac{\partial U}{\partial t} + \frac{\partial U}{\partial Y} = \frac{\partial P}{\partial X} + \frac{1}{Re} \left[1 + \frac{1}{\beta} \right] \frac{\partial^2 U}{\partial Y^2} - NmU - \frac{1}{\lambda} U - N_F U^2 \quad (6)$$

Energy Equation:

$$\frac{\partial \theta}{\partial t} + \frac{\partial \theta}{\partial Y} = \frac{1}{Pr Re} \frac{\partial^2 \theta}{\partial Y^2} + \frac{Ec}{\lambda} U^2 + N_F Ec U^3 \quad (7)$$

The transformed spatial boundary conditions now become:

$$At Y = -1: U = 0, \theta = -1 \quad (8a)$$

$$At Y = -1: U = 0, \theta = 1 \quad (8b)$$

Similar thermal boundary conditions (i.e. negative at one wall and positive at the other) were employed recently by Grosan and Pop (2007) in their study of fully-developed mixed radiative-convection in a vertical channel. The pressure gradient is decomposed into a steady component and an imposed (oscillatory) component as follows:

$$-\frac{\partial P}{\partial X} = \left(\frac{\partial P}{\partial X} \right)_s + \left(\frac{\partial P}{\partial X} \right)_o e^{i\omega t} \quad (9)$$

where $()_s$ is the steady component and $()_o$ is oscillating component. This approach had already been implemented extensively in pulsatile flow studies.

The heat flux at the upper plate may be written using Fourier's law as follows:

$$q_w = -k \frac{\partial h}{\partial y} \Big|_{y=1} = -\frac{k(h_2 - h_m)}{d} \theta' \quad (10)$$

where k is the coefficient of thermal conductivity.

The heat transfer coefficient is given by:

$$h_f = \frac{q_w}{(h_2 - h_m)} = -\frac{k}{d} \theta' \quad (11)$$

the Nusselt number can be written as:

$$Nu = \frac{h_f d}{k} = -\theta' \quad (12)$$

3. NUMERICAL SOLUTION BY THE FINITE ELEMENT METHOD

The transformed two-point boundary value problem defined by equations (6, 7) with boundary and

initial conditions (8a, b) has been solved using the finite element method (FEM). The authors have employed this technique successfully to simulate a wide range of non-Newtonian fluid dynamics problems. For example, Bhargava *et al.* (2007c) analyzed the reactive heat and mass transfer in micropolar-saturated Darcian porous media using finite elements. Bhargava *et al.* (2007d) also investigated the viscoelastic flow in a Darcy-Forchheimer porous medium with wall mass flux effects using the finite element method. FEM has been shown to be highly versatile and extremely accurate in fluid dynamics analysis. To solve the current coupled, nonlinear problem, we first redefine the pressure gradient as:

$$-\frac{\partial P^*}{\partial X} = P_s + P_o(\cos w^* t) \quad (13)$$

Using equation (10) the momentum equation (6) now becomes:

$$\begin{aligned} \frac{\partial U}{\partial t} + \frac{\partial U}{\partial Y} &= P_s + P_o(\cos w^* t) + \frac{1}{Re} \left[1 + \frac{1}{\beta} \right] \frac{\partial^2 U}{\partial Y^2} - \\ &NmU - \frac{1}{\lambda} U - N_F U^2 \end{aligned} \quad (14)$$

The initial *temporal* condition is defined as:

$$At t = 0 : U = 0, \theta = -1 \quad (15)$$

The whole domain is divided into a set of 82 *line elements* of equal width, each element being two-noded. A number of stages are inherent in the analysis. We consider these in turn now.

Variational Formulation:

The variational form associated with equations (14), (7) over a typical two-noded linear element (Y_e, Y_{e+1}) is given by:

$$\int_{Y_e}^{Y_{e+1}} w_1 \left\{ \frac{1}{Re} \left[1 + \frac{1}{\beta} \right] \frac{\partial^2 U}{\partial Y^2} - \frac{\partial U}{\partial Y} - NmU - \frac{1}{\lambda} U - N_F U^2 - \frac{\partial U}{\partial t} + P_s + P_o(\cos w^* t) \right\} dY = 0 \quad (16)$$

$$\int_{Y_e}^{Y_{e+1}} w_2 \left\{ \frac{1}{PrRe} \frac{\partial^2 \theta}{\partial Y^2} + \frac{Ec}{\lambda} U^2 + N_F Ec U^3 - \frac{\partial \theta}{\partial Y} - \frac{\partial \theta}{\partial t} \right\} dY = 0 \quad (17)$$

where w_1 and w_2 are arbitrary test functions and may be viewed as the variation in U and θ respectively.

Finite Element Formulation:

The finite element model may be obtained from equations (16)-(17) by substituting finite element approximations of the form:

$$U = \sum_{j=1}^2 U_j \psi_j, \theta = \sum_{j=1}^2 \theta_j \psi_j \quad (18)$$

With $w_1 = w_2 = \psi_i$ ($i = 1, 2$) where ψ_i are the shape functions for a typical element (Y_e, Y_{e+1}) and are defined thus:

$$\psi_1^{(e)} = \frac{Y_{e+1} - Y}{Y_{e+1} - Y_e}, \psi_2^{(e)} = \frac{Y - Y_e}{Y_{e+1} - Y_e} \quad Y_e \leq Y \leq Y_{e+1} \quad (19)$$

The finite element model of the equations for a typical element (Y_e, Y_{e+1}) thus formed is given by:

$$\begin{bmatrix} [K^{11}] & [K^{12}] \\ [K^{21}] & [K^{22}] \end{bmatrix} \begin{bmatrix} \{U\} \\ \{\theta\} \end{bmatrix} + \begin{bmatrix} [M^{11}] & [M^{12}] \\ [M^{21}] & [M^{22}] \end{bmatrix} \begin{bmatrix} \{U\} \\ \{\theta\} \end{bmatrix}$$

$$= \begin{bmatrix} \{F^1\} \\ \{F^2\} \end{bmatrix} \quad (20)$$

Where $[K^{mn}]$, $[M^{mn}]$, and $[F^m]$, ($m, n=1, 2$) are matrices of order 2×2 , 2×2 , and 2×1 , respectively. Also U_i and θ_i are derivatives of U_i and θ_i with respect to t . All these matrices may be defined as follows:

$$\begin{aligned} K_{ij}^{11} &= -\frac{1}{Re} \left[1 + \left(\frac{1}{\beta} \right) \right] \int_{Y_e}^{Y_{e+1}} \frac{d\psi_i}{dY} \frac{d\psi_j}{dY} dY \\ &\quad - \int_{Y_e}^{Y_{e+1}} \psi_i \frac{d\psi_j}{dY} dY \\ &\quad - Nm \int_{Y_e}^{Y_{e+1}} \psi_i \psi_j dY \\ &\quad - \frac{1}{\lambda} \int_{Y_e}^{Y_{e+1}} \psi_i \psi_j dY \\ &\quad b j b_k \bar{U}_1 \int_{Y_e}^{Y_{e+1}} \psi_i \psi_1 \psi_k dY \\ &\quad - N_F \bar{U}_1 \int_{Y_e}^{Y_{e+1}} \psi_i \psi_2 \psi_k dY \\ K_{ij}^{12} &= 0, \end{aligned}$$

$$\begin{aligned} K_{ij}^{21} &= \frac{E_c}{\lambda} \bar{U}_1 \int_{Y_e}^{Y_{e+1}} \psi_i \psi_1 \psi_j dY \\ &\quad + \frac{E_c}{\lambda} \bar{U}_2 \int_{Y_e}^{Y_{e+1}} \psi_i \psi_2 \psi_j dY + N_F E_c \bar{U}_1^2 \int_{Y_e}^{Y_{e+1}} \psi_i \psi_1^2 \psi_j dY \\ &\quad + N_F E_c \bar{U}_2^2 \int_{Y_e}^{Y_{e+1}} \psi_i \psi_2^2 \psi_j dY + N_F E_c \bar{U}_1 \bar{U}_2 \int_{Y_e}^{Y_{e+1}} \psi_i \psi_1 \psi_2 \psi_j dY \\ K_{ij}^{22} &= -\frac{1}{PrRe} \int_{Y_e}^{Y_{e+1}} \frac{d\psi_i}{dY} \frac{d\psi_j}{dY} dY - \int_{Y_e}^{Y_{e+1}} \psi_i \frac{d\psi_j}{dY} dY \end{aligned}$$

$$\begin{aligned} M_{ij}^{11} &= - \int_{Y_e}^{Y_{e+1}} \psi_i \psi_j dY, M_{ij}^{12} = M_{ij}^{21} = 0, M_{ij}^{22} = \\ &- \int_{Y_e}^{Y_{e+1}} \psi_i \psi_j dY, \end{aligned} \quad (21)$$

$$F_i^1 = -\frac{1}{Re} \left[1 + \left(\frac{1}{\beta} \right) \right] \left(\psi_i \frac{d\psi_j}{dY} \right)_{Y_e}^{Y_{e+1}} - \int_Y^{Y_e} \psi_i (P_s + P_o(\cos w^* t)) dY \quad (22)$$

$$F_i^2 = -\frac{1}{PrRe} \left(\psi_i \frac{d\theta}{dY} \right)_{Y_e}^{Y_{e+1}} \quad (23)$$

where $\bar{U} = \sum_{i=1}^2 \bar{U}_i \psi_i$ and each *element* matrix is of the order 4×4 . Following assembly of all the element equations we obtain a matrix of order 166×166 . This system of equations is *non-linear* and is linearized by incorporating the functions \bar{U} which are assumed to be known. After applying the given boundary conditions only a system of 162 equations remain then to be solved and this is performed iteratively by the Gauss-Seidel method maintaining an accuracy of 0.0005.

4. GRAPHICAL RESULTS AND DISCUSSION

Numerical simulations have been performed to study the effect of Reynolds number (Re), rheological parameter (β), Darcy number (λ), Forchheimer number (N_F), hydromagnetic parameter (Nm), Eckert number (Ec) and Prandtl number (Pr) on velocity, U , and temperature, θ profiles across the channel (Y) with time, t . To obtain physically realistic computations we assume blood ($\rho = 1050 \text{ kg m}^{-3}$) flows between plates located at distance $2H = 1 \times 10^{-2} \text{ m}$ with suction $V_o = 0.01 \times 10^{-2} \text{ ms}^{-1}$. For this data, transpiration Reynolds number Re is equal to 0.2(approx.). Characteristic values of μ , c_p , k are taken as $3.2 \times 10^{-3} \text{ Kgm}^{-1}\text{s}^{-1}$, $14.65 \text{ J Kg}^{-1} \text{ K}^{-1}$ and $2.2 \times 10^{-3} \text{ J m}^{-1}\text{s}^{-1} \text{ K}^{-1}$ respectively. Following this data we also specify $Pr = 21$ and $Ec = 6.2 \times 10^{-11}$ as default values in the computations. The Eckert number characterizes the amount of mechanical energy dissipated as thermal energy in the flow. The electrical conductivity (σ) of stationary blood has been quantified as 0.7 s m^{-1} (2004). Since the electrical conductivity of flowing blood is always greater than that of stationary blood, in the present study we elect to use a slightly higher value of 0.8 s m^{-1} and conductivity is assumed to be temperature-independent for simplicity. In our computations the default values of the control parameters are: Reynolds number (Re) = 0.2, non-Newtonian parameter (β) = 4, dimensionless angular frequency (ω^*) = 8, steady component of pressure gradient (Ps) = 8, pulsating amplitude (Po) = 5, Darcian parameter (λ) = 0.7, Forchheimer parameter (N_F) = 0.03 (which corresponds to very weak inertial effects), magnetic field (Nm) = 2.4, Eckert number (Ec) = 6.2×10^{-11} and Prandtl number (Pr) = 21, unless otherwise stated.

Table 1 Comparison of Finite Difference and Finite Element Computations

$Re = 0.2, \beta = 4, \omega^* = 8, Ps = 8, Po = 5, \lambda = 0.7, N_F = 0.03, Nm = 2.4, Ec = 6.2 \times 10^{-11}, Pr = 21$		
Y	U (at $t = 0.5$)	
Y	FEM	FDM
-1	0	0
-0.82927	0.078597	0.078457
-0.65854	0.14009	0.1398
-0.48781	0.186385	0.186265
-0.31707	0.218782	0.218692
-0.14634	0.238059	0.238019
0	0.244384	0.244371
0.146341	0.241237	0.241215
0.317073	0.225167	0.22501
0.487805	0.194837	0.194359
0.658537	0.148762	0.148213
0.829268	0.08480	0.08362
1	0	0

Table 2 Values of $\theta'(1)$ for different values of Re and Pr

$$\left(\beta = 4, \omega^* = 8, Ps = 8, Po = 5, \lambda = 0.7, N_F = 0.03, Nm = 2.4, Ec = 6 \times 10^{-11} \right)$$

Re ($Pr = 21$)	$-\theta'(1)$	Pr ($Re = 0.2$)	$-\theta'(1)$
0.05	2.858958	0.5	1.102009
0.2	8.60861	1	1.214391
0.3	12.16511	5	2.758221
0.5	18.8678	10	4.683559

In order to access the accuracy of our results, comparisons have been made with the finite difference method (details of which are provided in previous studies by the authors, for example (2009) and results are shown in Table 1. Excellent correlation can be observed between both methods for the dimensionless velocity profile (U) with transverse coordinate (Y), while in Table 2, the variation of heat transfer for the different value of Re and Pr is tabulated

Spatial-temporal variations of the velocity and temperature fields for various flow cases are shown in figures 2 (a)-(b), figure 3 and figure 4 respectively. The complete detail study are given below.

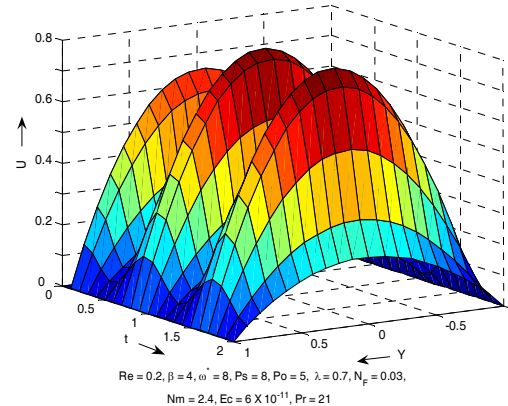


Fig. 2a. Non-Dimensional velocity profile (U) versus transverse coordinate (Y) and time (t) for the general magneto-bio-rheological, non-Darcian case.

Figures 2(a) and 2(b) depict the velocity, U and temperature, θ , profiles with respect to both space Y and time t for the general flow case. In figure 2a the oscillatory nature of the flow is clear with peak velocities always corresponding to the centre of the channel. With increase in time, the magnitude of these peaks is increased. On the other hand in figure 2b the temperature (θ) distribution is *not oscillatory* in nature and descends smoothly for all time, from a maximum of 1 at the upper plate ($Y = 1$) to -1 at the lower plate ($Y = -1$).

The spatial-temporal distribution of velocity, U for the Newtonian case ($\beta \rightarrow \infty$) is depicted in figure 3. It is immediately apparent when comparing the oscillatory profile with the general rheological case (figure 2a) that the peak velocities are increased for all time. Peak velocities for the non-Newtonian case ($\beta = 4$) are approximately 0.24, 0.58 and 0.67 corresponding to $t = 0.5, 1$ and 1.5 ; for the Newtonian case (fig. 3) these values are boosted to 0.29, 0.71 and 0.77 approximately. The rheological

nature of the biofluid (*greater for smaller values of β*) therefore decelerates the flow velocity at the channel centre i.e. the peak velocities of the Newtonian fluid are always greater compared with the bio-rheological fluid, even in the presence of a magnetic field.

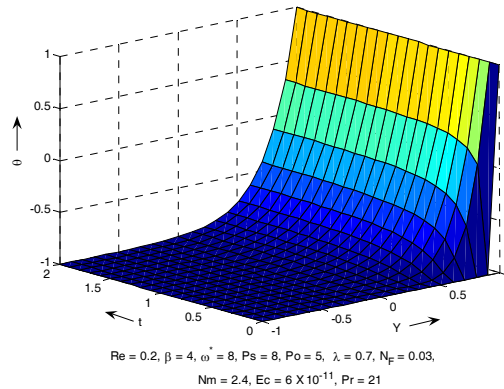


Fig. 2b. Non-Dimensional temperature profile (θ) versus transverse coordinate (Y) and time (t) for the general magneto-bio-rheological, non-Darcian case.

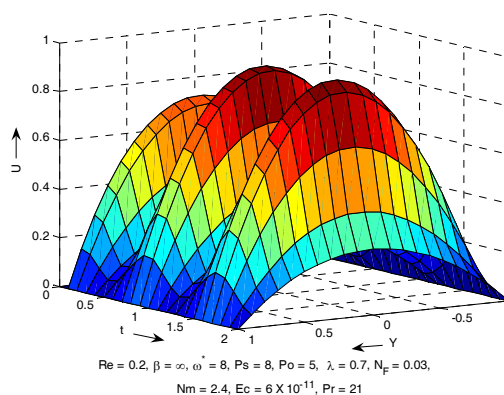


Fig. 3. Non-dimensional velocity profile (U) versus transverse coordinate (Y) and time (t) for Newtonian, MHD, non-Darcian case (i.e when $\beta \rightarrow \infty$).

In fig. 4 the velocity profile for the purely fluid (rheological) case ($\lambda \rightarrow \infty$ and $N_F=0$) is also seen to have greater peak values in the vicinity of the channel centre ($Y = 0$) for all times computed, compared with the general non-Darcian case (figure 2a), although the increase is less pronounced than for the Newtonian case (fig. 3). The presence of porous drag forces therefore clearly decelerates the flow i.e. reduces velocity values.

In fig. 5 to 11, spatial distributions of temperature and velocity have been presented, each at $t = 0.5$, for variation of different control parameters in the model.

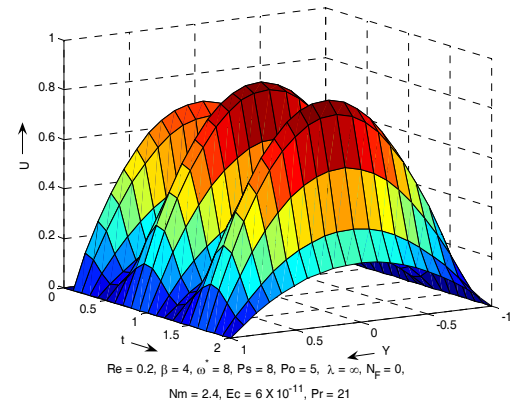


Fig. 4. Non-dimensional velocity profile (U) versus transverse coordinate (Y) and time (t) for MHD, rheological, non-porous case (i.e when $\lambda \rightarrow \infty$ and $N_F = 0$).

Figure 5 shows the influence of the transpiration Reynolds number on velocity profile at time $t = 0.5$. As expected, an increase in Reynolds number from 0.05 to 1 boosts the fluid velocity i.e. accelerates flow across the channel. The profiles although generally parabolic are increasingly skewed to the right i.e. towards the upper plate ($Y = 1$), with an increase in Re since this parameter incorporates the suction velocity (V_o) i.e. with greater Re values suction at the upper plate will be enhanced which will serve to displace the velocity distribution towards the upper plate.

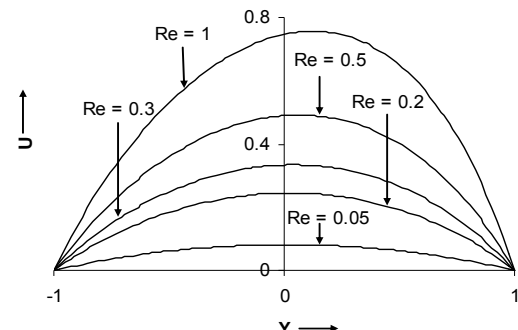


Fig. 5. U versus Y for various transpiration Reynolds numbers (Re) at $t = 0.5$.

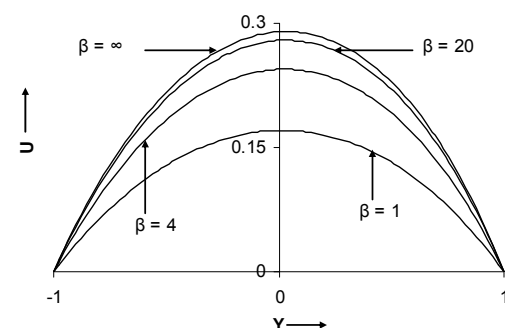


Fig. 6. U versus Y for various non-Newtonian parameter values (β) at $t = 0.5$.

Figure 6 illustrates the influence of rheological parameter, β , on fluid velocity at time $t = 0.5$.

Smaller value of this parameter correspond to *stronger non-Newtonian behaviour* (i.e. a rise in the viscosity) which will decelerate the flow and reduce longitudinal fluid velocity, U . $\beta \rightarrow \infty$ represents the case of a Newtonian fluid which corresponds to the *lowest* value of fluid viscosity and contributes to the *maximum* velocity computed. $\beta = 1$ corresponds to strongly rheological flow at higher viscosity and results in the minimization of fluid velocity, U across the channel.

In fig. 7 the influence of Darcy parameter on velocity profile is shown, again for the general magneto-rheological case. As the Darcy parameter, λ , is directly proportional to permeability, a rise in λ therefore implies an increase in permeability. A corresponding decrease in matrix fibers of the porous medium therefore occurs. Such fibers may take the form of blockage debris, tumors or fatty deposits in biomedical scenarios. Reduction in the presence of such materials will manifest in a reduction in the Darcian drag force, $-U/\lambda$, in equation (11) which will decrease the resistance to the flow, resulting in an acceleration of the biofluid i.e. increase in velocity, U . Peak velocity falls from approximately 0.26 for $\lambda = 5$ (high permeability, low Darcian drag) to 0.17 for $\lambda = 0.1$ (low permeability, high Darcian drag).

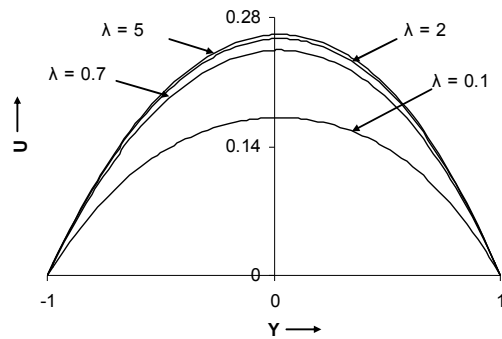


Fig. 7. U versus Y for various Darcian parameter values (λ) at $t = 0.5$.

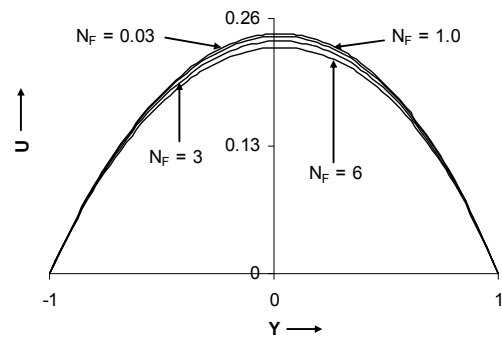


Fig. 8. U versus Y for various Forchheimer parameter values (N_F) at $t = 0.5$.

The effects of Forchheimer quadratic drag parameter, N_F , on the velocity profile across the channel are shown in figure 8. An increase in N_F , leads to an increase in Forchheimer quadratic drag, i.e. the term $-N_F U^2$ in equation (11), which acts to resist the flow in the channel and to decrease

velocities. Peak velocity falls from approximately 0.245 near the channel centre line ($\sim Y = 0.5$) for $N_F = 0.03$ to 0.23 for $N_F = 6$.

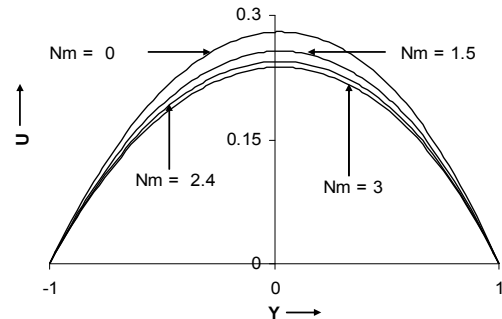


Fig. 9. U versus Y for various hydromagnetic parameter values (N_m) at $t = 0.5$.

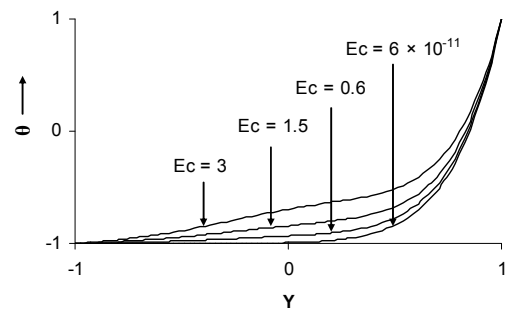


Fig. 10. θ versus Y for various Eckert numbers (E_c) at $t = 0.5$.

Figure 9 depicts the effect of hydromagnetic parameter, N_m , on velocity profile at time $t = 0.5$. As N_m increases, there is a decrease in the velocity of bio-rheological fluid due to the increase in the retarding force (Lorentz body force) generated by the magnetic field. This trend is in excellent agreement with the Newtonian fluid results presented by Mekheimer (2000) indicating that even in strongly non-Newtonian flow ($\beta = 4$), magnetic field depresses blood flow.

Figure 10 shows the influence of Eckert Number E_c on temperature profile at time $t = 0.5$. E_c quantifies the ratio of kinetic energy of the flow to the enthalpy difference. For very low E_c values i.e. 6.2×10^{-11} , very little mechanical energy is dissipated as heat in the fluid i.e. no warming effect occurs throughout the entire lower semi-section of the channel ($-1 < Y < 0$) where temperatures remain negative. The negativity of temperature is forced by the lower boundary condition ($\theta = -1$ at $Y = -1$ in 8a). This negative temperature behavior is sustained throughout most of the upper semi-section of the channel also ($0 < Y < 0.9$) until temperatures cross-over very close to the upper heated plate at $Y \sim 0.9$. No flow reversal has been computed in our case although such an effect has been reported for the case of a moving wall by Gschwendtner (2004). But for higher E_c values ($E_c = 3$) we observe that there is a considerable increase in the temperature profiles as depicted by Fig. 10. This effect is clearly absent at the very low values of E_c since the viscous heating term has negligible effect at these

values.

Finally in figure 11 the effect of Prandtl number on temperature profiles (θ) is illustrated. Pr represents the ratio of momentum diffusivity to thermal diffusivity. Larger Pr fluids ($Pr > 1$) will diffuse momentum faster than heat. For $Pr = 1$ the momentum and energy will be diffused at the same rate. Increasing Pr from 1 through 5, 10 and 21 therefore will decrease temperatures of the biofluid in the channel, as observed in figure 11. In consistency with the spatial boundary conditions temperatures ascend from the minimum value of -1 at the lower plate to the maximum value of 1 at the upper plate.

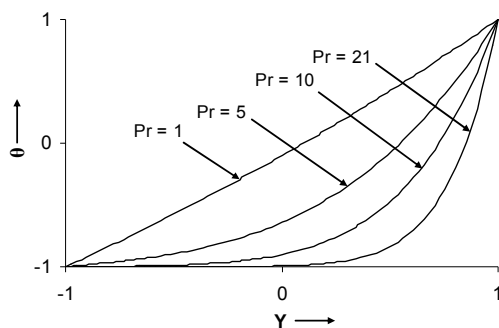


Fig. 11. θ versus Y for various Prandtl numbers (Pr) at $t = 0.5$.

5. CONCLUSIONS

In the present study, the pulsatile magneto-rheological blood flow through a horizontal channel containing a porous medium in the presence of a transverse magnetic field and viscous heating present has been analyzed numerically using the finite element method. Numerical results have shown that an increase in Darcy parameter (λ), transpiration Reynolds number (Re) and rheological parameter (β) accelerates the fluid flow, whereas fluid velocity is reduced with an increase in Forchheimer (quadratic porous drag) parameter and hydromagnetic number. A major increase is observed in temperature profile for high Eckert numbers, which is absent when Ec is small. The results indicate that the magnetic field has a considerable effect on the velocity profile as does the porous medium and the biofluid rheology. The current findings warrant further investigations where the magnetic field is non-uniform and where Joule heating effects are present. Results relating to such efforts will be communicated in the near future.

REFERENCES

- Bég, O. A., H. S. Takhar, R. Bhargava, S. Sharma and T. K. Hung (2007). Mathematical modeling of biomagnetic flow in a micropolar-fluid saturated Darcian porous medium. *Int. J. Fluid Mechanics Research* 34(5), 403-424.
- Bég, O. A., T. A. Bég, R. Bharagava, Rawat, S., H. S. Takhar and T. K. Hung (2007). Numerical analysis of biomagnetic Newtonian flow in a Darcy-Forchheimer porous medium. *J. Theoretical and Applied Mechanics* 32(3), 20-45.
- Bhargava, R., H. S. Takhar, S. Rawat, Tasveer A. Beg and O. Anwar (2007). Beg, Finite element solutions for non-Newtonian pulsatile flow in a non-Darcian porous medium conduit, *Nonlinear Analysis: Modelling and Control*, 12(3), 317-327.
- Bhargava, R., S. Rawat, H. S. Takhar and O. A. Bég (2007). Pulsatile magneto-biofluid flow and mass transfer in a non-Darcian porous medium channel. *Meccanica* 42, 247-262.
- Bhargava, R., S. Rawat, H. S. Takhar, T. A. Bég and O. A. Bég (2007). A study of buoyancy-driven micropolar heat and mass transfer in a Darcian porous regime with chemical reaction, *Nonlinear Analysis: Modelling and Control* 24(1), 1-24.
- Bhargava, R., S. Sharma, H. S. Takhar, O. A. Bég and P. Bhargava (2007). Numerical Solutions for Micropolar Transport Phenomena over a Nonlinear Stretching Sheet, *Nonlinear Analysis: Modelling and Control* 12(1), 45-63.
- Chattopadhyay, H., F. Durst and S. Ray (2006). Analysis of heat transfer in simultaneously developing pulsating laminar flow in a pipe with constant wall temperature. *Int. Comm. Heat and Mass Transfer* 33(4), 475-481.
- developed mixed convection flow in a vertical channel.
- Gabrial, S., R. W. Lau, C. Gabrial (2004). The dielectric properties of biological tissues: III. Parametric models for the dielectric spectrum of tissues. *Phys. Medicine Biol.* 41, 2271-2293.
- Ghazian, O. and H. Rezvantabar (2011). Mehdi Ashjaee., Analytical Investigation of the Effect of Viscous Dissipation on Couette Flow in a Channel Partially Filled with a Porous Medium. *Transport in Porous media* 89(1), 1-13.
- Grosan, T. and I. Pop (2007). Thermal radiation effect on fully Technische. *Mechanik* 27(1), 37-47.
- Gschwendtner, M. A. (2004). The Eckert number phenomenon: Experimental investigations on the heat transfer from a moving wall in the case of a rotating cylinder. *Heat Mass Transfer*, 40(6-7), 551-559.
- Ibrahim, A. A., M. F. El-Amin and A. Salama (2009). Effect of thermal dispersion on free convection in a fluid saturated porous medium. *International Journal of Heat and Fluid Flow* 30(2), 229-236.
- Ildoskey, I. M. (2012). Slip effect on the unsteady MHD pulsatile blood flow through porous medium in an artery under the effect of body acceleration.
- Kairi, R. R. and P. V. S. N. Murthy (2011). Effect of

- viscous dissipation on natural convection heat and mass transfer from vertical cone in a non-Newtonian fluid saturated non-Darcy porous medium. *Applied Mathematics and Computation* 217(20), 8100-8114.
- Khaled, A. R. A. and K. Vafai (2003). The role of porous media in modeling flow and heat transfer in biological tissues. *Int. J. Heat and Mass Transfer* 26(46), 4989-5003.
- Loukopoulos, V. C. and E. E. Tzirtzikakis (2004). Biomagnetic channel flow in spatially varying magnetic field. *Int. J. Engineering Science* 42(5-6), 571-590.
- Madjalani, J. and H. A. Chibli (2002). Pulsatory channel flow with arbitrary pressure gradients. *AIAA 3rd Theoretical Fluid Mechanics Meeting*, St. Louis, MO, USA 24-26 June.
- Mahdy, A. and J. Chamkha (2010). Chemical reaction and viscous dissipation effects on Darcy-Forchheimer mixed convection in a fluid saturated porous media. *International Journal of Numerical Methods for Heat & Fluid Flow* 20(8), 924-940.
- Mekheimer, K. S. (2004). Peristaltic flow of blood under effect of a magnetic field in a non-uniform channel. *Applied Mathematics and Computation J.* 153(3), 763-777.
- Misra, J. C., J. C. Sheet and H. J. Rath (2008). Flow and heat transfer of a MHD viscoelastic fluid in a channel with stretching walls: Some applications to haemodynamics. *Computers and Fluids* 37(1), 1-11.
- Nadeem, S., N. S. Akbar, T. Havat and A. A. Hendi (2012). Influence of Heat and Mass Transfer on Newtonian Biomagnetic Fluid of Blood Flow Through a Tapered Porous Arteries with a Stenosis. *Transport in Porous media* 91(1), 1-13.
- Ogulu, A. (2006). Effect of heat generation on low Reynolds number fluid and mass transport in a single lymphaticblood vessel with uniform magnetic field, *Int. Comm. Heat and Mass Transfer* 33(6), 790-799.
- Ogulu, A. and E. Amos (2007). Modeling pulsatile blood flow within a homogeneous porous bed in the presence of a uniform magnetic field and time-dependent suction. *Int. Comm. Heat Mass Transfer* 34, 989-995.
- S. Rawat, R. Bhargava and O. Anwar (2010). Bég, Hydromagnetic micropolar free convection heat and mass transfer in a darcy forchheimer porous medium with thermophysical effects : Finite element solution. *Int. J. of Appl. Math and Mech.* 6(13), 72-93.
- Takhar, H. S., R. Bhargava, S. Rawat, T. A. Bég and O. A. Bég (2007). Finite element modeling of laminar flow of a third grade fluid in a Darcy-Forchheimer porousmedium withsuction effects. *Int. J. Applied Engineering*, 12(1), 215-233.
- Tenforde, T. S. (2005). Magnetically-induced electric fields and currents in the circulatory system. *Progress in Biophysics Molecular Biology* 87(2-3), 279-288.
- Voltairas, P. A. (2002). Fotidis D. I. and Michalis L. K., Hydrodynamics of magnetic drug targeting. *J. Biomechanics* 35, 813.